Lawrence Berkeley National Laboratory

Lawrence Berkeley National Laboratory

Title

Relationship Between Atmospheric circulation and Snowpack in the Western United States

Permalink

https://escholarship.org/uc/item/9443g18j

Authors

Jin, Jiming
Miller, Norman L.
Sorooshian, Soroosh
et al.

Publication Date

2008-06-04

Peer reviewed

Relationship Between Atmospheric Circulation and Snowpack in the Western United States

Jiming Jin* and Noman L. Miller

Earth Sciences Division, University of California-Berkeley National Laboratory

Soroosh Sorooshian and Xiaogang Gao

Department of Civil and Environment Engineering, University of California, Irvine, California

* Corresponding Author: Jiming Jin

JimingJin@lbl.gov

90-1116 One Cyclotron Road

Earth Sciences Division,

Berkeley National Laboratory, Berkeley, CA 94720

Relationship Between Atmospheric Circulation and Snowpack in the Western United States

Jiming Jin and Noman L. Miller

Earth Sciences Division, University of California-Berkeley National Laboratory

Soroosh Sorooshian and Xiaogang Gao

Department of Civil and Environment Engineering, University of California, Irvine, California

Abstract

Snow anomalies in the western United States (U.S.) have been widely investigated by many researchers due to its impact on water availability. This study focuses on how anomalous atmospheric circulation affects snowpack accumulation in the western U.S. using observations and output from the National Center for Atmospheric Research (NCAR) Community Climate Model version 3 (CCM3). Our results indicate that the mid-latitude atmospheric circulation anomalies induced by the El Nino-Southern Oscillation (ENSO) tend to drive winter precipitation shifts, leading to an anomalous snowpack distribution in the western U.S. The warm phase of ENSO produces increased snowpack in the Southwest, while the cold phase of ENSO generates increased snowpack in the Northwest. Temperature has a secondary impact on the anomalous snowpack distribution during ENSO episodes. Additionally, the non-linear atmospheric dynamics-related Pacific-North American (PNA) pattern is found to strongly affect snow anomalies in the western U.S. independent from ENSO. The positive phase of the PNA pattern produces colder temperature and stronger precipitation due to the lower pressure in the region, leading to an above normal snowpack. Conversely, the negative phase of the PNA pattern generates warmer temperature and weaker precipitation resulting from the higher pressure, producing a below than normal snowpack in the western U.S. In general, the NCAR-CCM3 reproduces the observed processes. However, model biases are identified and reported. The information provided in this study strengthens our understanding of climate and water supply variability in the western U.S.

1. Introduction

Studies of the relationship between interannual climate variability and snowpack characteristics as well as the importance of snow in the Western United States (WUS) to water supply have been addressed by many researchers (e.g. Redmond and Koch 1991; Serreze et al. 1999; McCabe 1996; Clark et al 2001; McCabe and Dettinger 2002). Using principal component analysis (PCA), Cayan (1996) studied the effects of large-scale atmospheric circulation on the WUS April 1 snowpack, a time when snowpack usually reaches its maximum value (McCabe 1996; Clark et al. 2001). Cayan found that the first five PCA components of the snowpack in the WUS are related to different atmospheric circulation patterns. McCabe and Dettinger (2002) indicated that two PCA primary modes of the atmospheric circulation, driven by El Nino-Southern Oscillation (ENSO) and Pacific Decadal Oscillation (PDO), account for 61% of the total snowpack variability. Redmond and Koch (1991) found that during the WUS snow accumulation period, the South Oscillation Index (SOI) and Pacific-North America (PNA) index are strongly correlated with precipitation and temperature, which are two critical variables affecting snow accumulation and depletion rates (Hamlet and Lettenmaier 2004 submitted to Journal of Climate), indicating that variations in the atmospheric circulation significantly contributes to WUS snow mass amounts.

As such, understanding the mechanisms of mid-latitude atmospheric circulation variations is crucial to WUS snow anomaly forecasting. Lau and Nath (1994) used an Atmospheric General Circulation Model (AGCM) to investigate the impact of the tropical Pacific Sea Surface Temperature (SST) on the mid-latitude atmospheric circulation. They found that the AGCM, forced by ENSO-like tropical Pacific SSTs, produce anomalous atmospheric

3

patterns similar to the patterns observed during ENSO episodes. They also found that extratropical SST anomalies have minor effects on the mid-latitude atmospheric circulation. Strous and Shukla (2002) analyzed the anomalous mid-latitude atmospheric patterns based on both AGCM simulations and observations. Their findings indicate that under the neutral SST condition, the mid-latitude atmosphere has strong anomalies, with patterns that differ from AGCM simulations forced by tropical Pacific SSTs during ENSO episodes. These anomalous atmospheric patterns under the neutral SST condition can be attributed to nonlinear atmospheric dynamics (i.e. atmospheric internal variability), defined as Pacific-North American (PNA) patterns in Strous and Shukla (2002) based on the 500 mb geopotential heights.

It is of great interest to investigate the characteristics of snowpack variations in the WUS and related processes as forced by ENSO SSTs and nonlinear atmospheric dynamics. According to Strous and Shukla (2002)'s work, the present study provides a reclassification of ENSO and PNA based on observations and model output. This study provides an evaluation of the detailed physical processes between anomalous atmospheric circulation and snowpack variation in the WUS. Additionally, this paper includes an evaluation of snowpack simulations within the National Center for Atmospheric Research (NCAR) Climate Community Model version 3 (CCM3) coupled to a sophisticated snow scheme (Jin et al. 1999).

This study strengthens our understanding of climate variability, improving forecasts of WUS climate and water resources. In Section 2, the data and model used are described. Section 3 provides definitions of ENSO and PNA, and Section 4 discusses WUS snow anomalies. Analyses of the impact of ENSO on snowpack are provideds in Section 5. Section 6 investigates the impact of PNA patterns on the snowpack, and Section 7 evaluates the CCM3 snow anomaly simulations for the WUS., and discussions and conclusions are given in Section 8.

2. The Data and Model:

In this study, the Snow Water Equivalent (SWE) depths for the WUS are from snow course data collected manually by the U.S. Department of Agriculture (USDA) cooperative snow survey program and the California Department of Water Resources. This dataset is based on more than 2,000 permanent sites in the WUS, where measurements are made on the first day of each month from January to June since the mid-1940s. The April 1 SWE represents the annual snowpack maximum value (McCabe 1996; Bohr and Aguado 2001), and is a focus of the present analysis. This analysis used 246 snow course stations out of more than 2,000 stations which are roughly evenly distributed over the WUS. Each station has at least 25 years of effective April 1 SWE data between 1950 and 1997. The SST and 500mb data were from the Centers for Environmental Prediction/National Center for Atmospheric Research (NCEP/NCAR) Reanalysis during the November to March snow accumulation period from 1950 to 1997. The observed $1^o \times 1^o$ precipitation and 2-m height air temperature for 1950 through 1997 were obtained from Legates and Willmott (1996a,b).

Numerical simulations were generated using the NCAR CCM3. This model has 18 vertical atmospheric levels extending from the surface boundary layer to the 2.9mb level and a horizontal resolution of approximately $2.8^o \times 2.8^o$. In the present study, the CCM3 land surface model (Bonan 1996) was replaced by the Snow-Atmosphere-Soil Transfer (SAST) model (Jin et al. 1999), as it has a more advanced snow scheme. SAST has 3 snow layers and 10 soil layers which simulate water and heat transfer within snow and soil. The vegetation scheme in SAST is based on Dickinson et al. (1993). Our coupled CCM3-SAST was used to produce a December

1949 to May 1995 simulation, where the NCAR/NCEP SSTs were used as the lower boundary condition over the oceans.

3. ENSO and PNA definitions

The Niño 3.4 SST index defined by Trenberth (1997) is the spatially averaged SST for 120 ^{o}W-170 ^{o}W and 5 ^{o}S-5 ^{o}N. In this study, the winter Niño 3.4 SST was temporally averaged for December to February (DJF) to identify ENSO events. When the SST standard deviation is above 1°C, below -1°C, or between -1°C and 1°C, the winter is defined as "warm", "cold", or "normal", respectively, which follows the definitions of Straus and Shukla (2002). For the 1950-1997 study, there are 8 warm, 6 cold, and 33 normal winters (see Table 1).

The PNA index originally as defined by Wallace and Gutzler (1981), has the following formula:

$$PNA = 0.25 \, [Z(20^{o}N, 160^{o}W) - Z(45^{o}N, 165^{o}W) + Z(55^{o}N, 115^{o}W) - Z(30^{o}N, 85^{o}W)]. \qquad (1)$$

Z represents the standardized 500mb geopotential height at the prescribed latitude and longitude. The PNA indices for DJF were averaged to identify winter PNA patterns. In order to eliminate the effects of the tropical Pacific Ocean, the Eq. (1) was only applied to the 33 neutral winters. When the DJF-averaged index is above 0.5, the PNA pattern is defined as "positive", and when it is below -0.5, the PNA pattern is "negative". Statistical results for the 1950-1997 indicate that ±0.27 are the lower and upper limits of a 99% Student t test for the PNA index. As such, a significant PNA pattern can be identified when the index is outside the range ±0.5. Based on this definition, there are 9 positive and 6 negative PNA periods for the 33 neutral winters (Table 1).

4. SWE anomalies and EOF analysis

4.1 SWE anomalies

Observational and modeling studies have indicated that the global warming significantly reduces the WUS snow cover (e.g. Roos 1986; Dettinger and Cayan 1995; Miller et al. 2003). The values of the WUS-spatially averaged April 1 SWEs for 1951 to 1997 are shown in Fig. 1. The linear regression shows a decreasing trend during this near 5-decade period, with more than a 6cm SWE reduction over the WUS. Thus, in order to accurately interpret the WUS SWE anomalies, the time series for each snow course station was detrended. The station SWEs were interpolated to the 1^ox1^o resolution using a natural neighbor gridding package developed by Watson (1999). The interpolated anomalous April 1 SWE composites for the warm ENSO, cold ENSO, positive PNA, and negative PNA are shown in Fig. 2 and the sample number for each composite is given in Table 1.

The warm ENSO composite (Fig. 2a) indicates that positive SWE anomalies are very dominant in the southwestern U.S., with a maximum value greater than 160 mm. Portions of the Northwest region, such as the coastal region and parts of Washington, Oregon, and Idaho, also have positive anomalies, but are below the 95% significance level. Negative SWE anomalies are significant in parts of Idaho, Montana, Wyoming, as well as northern Colorado, but weak and unsystematic, when compared to the positive pattern in the Southwest. The cold ENSO produces strong positive SWE anomalies in most of the Northwest (Fig. 2b), but generates weak negative anomalies in the Southwest, which are mostly below the 95% significance level. It is clearly seen that the warm ENSO has a strong impact on the SWE in the Southwest, while the cold ENSO produces a dominant effect in the Northwest.

7

Fig. 2c shows that the strong negative SWE anomalies cover the entire WUS under the positive PNA pattern. However, during the negative PNA, the positive SWE anomalies are dominant in the WUS, except for some insignificant negative values in the coastal region of the Northwest (Fig. 2d). The maximum absolute SWE value for the positive PNA pattern is over 240 mm compared to less than 200 mm under the negative PNA pattern. The total area for the above significant level of the SWE under the positive PNA pattern is also larger (Fig 2c and d), suggesting that the positive PNA pattern contributes significantly more to the SWE variations than the negative PNA pattern in the WUS.

4.2 EOF analysis of the SWE anomalies

The above analysis indicates that the PNA and ENSO induced SWE anomalies are dramatically different, and that these two kinds of processes cause significant SWE anomalies in the WUS. In order to quantify the contribution of each process to the snow variations, Empirical Orthogonal Function (EOF) analysis was applied to the observed SWEs at the 246 selected snow course stations. The loadings at each station were interpolated to 1° x 1° grids (Fig 3). The combined variance for the first two EOF components explains about 57% of the total SWE variance, where the first component (EOF-1) explains 39%, and the second (EOF-2) explains 18%.

The EOF-1 loadings strongly resemble the PNA pattern related SWE anomalies, indicating that the signs of the SWE anomalies in the WUS are consistent. The EOF-1 pattern bears more characteristics of the SWE anomalous pattern under the positive PNA than those under the negative PNA. For example, three lower SWE centers located on the coast and the

southeast boundary of Washington, and the northeast boundary of California (Fig. 2c), correspond to three high centers on the loading map at the same locations as in Fig. 3a. This indicates that the lower SWE under the positive PNA pattern has a larger contribution to the SWE variance for the EOF-1 than the higher SWE under the negative PNA pattern.

The EOF-2 loadings resemble the ENSO produced SWE anomalies (Fig. 3b), with the discrepancy that the zero anomaly line shifts slightly to the north when compared to the two ENSO-related anomalous snow patterns. The positive loadings strongly resemble the higher SWE distributions in the Southwest produced by the warm ENSO (Fig. 2a), while the negative loadings are similar to the deeper SWEs in the Northwest generated by the cold ENSO (Fig. 2b). The geographic distribution of the EOF-2 loadings apparently is a combination of the positive SWE anomalies from both Figs. 2a and b. For example, high values are seen in the Sierra Nevada area of California in both Fig. 2a and Fig. 3b, while two high centers located in Washington and Idaho (Fig. 2b) correspond to two low centers in Fig. 3b at the same locations. Therefore, the SWE EOF-1 pattern with 39% of the total variance explained represents the PNA-produced SWE anomalies, and the EOF-2 pattern with 18% of the total variance explained represents the ENSO-produced SWE anomalies. This EOF analysis indicates that PNA-related atmospheric processes more significantly impact the SWE anomalies than the ENSO-related processes. This finding suggests that the understanding of snow mass variations in the WUS need to consider effects of both non-linear atmospheric dynamics (PNA) and tropical Pacific SSTs. If it is solely based on ENSO, then WUS snow mass predictions would result in large errors.

5 Impact of ENSO on snowpack in the WUS

Studies have shown that ENSO alters the mid-latitude atmospheric circulation (Lau and Nath 1994; Livezey and Mo 1987), which results in WUS climate variability. Here we examine variations in precipitation and temperature during ENSO episodes in order to understand the anomalous SWE patterns, since SWE anomalies in the WUS are strongly related to these two variables (Cayan 1996).

5.1 Precipitation and Temperature

Snow mass accumulation is inherently linked to temperature, precipitation rates, and precipitation type (rain or snow). In the WUS winter, roughly 50-70% of precipitation falls as snow. Temperature controls not only the precipitation type, but also snowmelt rate (i.e. as a result of the snowmelt rates, a warmer winter is linked to less snowpack and a colder winter is linked to more snowpack).

In this study, composite precipitation and temperature anomalies for warm and cold ENSO episodes during 1950-1997 were averaged for the November through March snow accumulation period (Fig. 4). During the warm ENSO, the precipitation pattern in the WUS is very similar to the SWE pattern. The zero anomaly line demarking the positive and negative precipitation anomalies are consistent with that on the SWE map. The strong positive precipitation anomalies in the Southwest produce the increased SWE during the snow accumulation period. On the other hand, the reduced precipitation over Montana, parts of Wyoming, and northern Colorado, result in decreased SWE, which pass the 95% significance test. Although a significant low precipitation center occurs in western Washington, the corresponding shallow SWEs are below the significance level, implying that the type of the precipitation and/or local factors play a contributing role in this phenomenon. In the meantime,

the temperature pattern, to some extent, is consistent with the SWE pattern during the warm ENSO, but the zero anomaly temperature line is about 2° latitude south of the positions of the zero anomaly lines for the SWE and precipitation. Clearly, the lower temperatures combined with stronger precipitation in the Southwest contributes to the increased SWE, and the higher temperatures overlapping with the weaker precipitation in the Northwest contributes to the decreased SWEs. However, in eastern Washington and Oregon, the stronger precipitation is consistent with the deeper SWE, but the corresponding higher temperatures in this same region do not turn the positive SWE anomalies to negative values. This evidence, in addition to the similarity between the precipitation and SWE patterns, implies that precipitation plays a more critical role in determining SWE conditions during the warm ENSO than the temperature.

During the cold ENSO episodes, the precipitation pattern is also consistent with the SWE pattern. The stronger precipitation produced the deeper SWE in most of the Northwest, especially along the coast. The position of the zero anomaly precipitation line is in good agreement with that for the SWE. In the Southwest, although the reduced precipitation apparently produces decreased SWE, the SWE anomalies do not pass the 95% significance level in most areas, implying that other factors also affect the SWE. However, the temperature pattern is not compatible with the SWE pattern. The colder climate prevails in most of the West, and the zero temperature anomaly line shifts dramatically to the southeastern corner of the West, compared to that for the SWE or precipitation. In most parts of New Mexico and some areas in Arizona and Colorado, the temperature anomalies show significant positive values (Fig.4d). The inconsistency between the temperature and SWE patterns suggests that during cold ENSO episodes, the temperature has a weaker influence on the SWE anomalies than the precipitation. Thus, ENSO changes the normal precipitation patterns in the WUS, leading to the SWE

11

anomalies, while the ENSO induced anomalous temperature patterns have a secondary effect on the snowpack.

4.2 500mb geopotential height anomalies during the ENSO episodes

As we know, the ENSO related atmospheric circulation anomalies in the mid-latitudes lead to climate variability in the WUS (Cayan 1996; McCabe and Dettinger 2002). These anomalies change the way moisture is transported, leading to the precipitation variability in the WUS. In this subsection, the connections between the anomalous atmospheric circulation and variations in precipitation and snowpack are investigated during the ENSO events.

Fig 5a shows the 500mb geopotential height anomaly map during the warm ENSO, where a strong zonally-oriented high is centered east of Canada, and a low centered in the northeastern Pacific Ocean extends through the southern U.S. to the Atlantic Ocean. A zero height anomaly line demarking highs and lows over the West crosses northern Colorado, the southwest corner of Wyoming, and the boundary of Idaho and Montana. The thick dashed line in Fig. 5a represents the position of the climatological 500mb geopotential height ridge in the Pacific-North America sector during the snow accumulation period. This ridge is located along the Northwest coast, north of 42°N, with a north-south orientation, and extends southwestwardly to the Pacific Ocean. The intensity of this ridge is critical to determination of the precipitation patterns in the WUS. Table 2 shows the latitudinal changes in the magnitude of this climatological ridge during the ENSO. During the warm ENSO, the southern part of the ridge in the ocean is significantly weakened by the low over the North Pacific (Fig. 5a). This weakening strengthens atmospheric moisture transport from the ocean to the Southwest, resulting in intensified precipitation during the warm ENSO (Fig. 4a). The north part of the ridge near the

12

Northwest coast has only a slight decrease because of the weak geopotential height anomalies. This causes a small variation in the atmospheric moisture transport to the Northwest, but does not lead to a dramatic precipitation change as was found in the Southwest. The Northwest can be divided into two sub-regions by the zero geopotential height anomaly line. The east part is covered by the high, which heightens the pressure over the region. The heightened pressure encourages downdrafts in the atmosphere and decreases the precipitation in the region. The west part of the zero anomaly line is covered by the low, which weakens the high pressure ridge. Theoretically, the lowered pressure would increase the precipitation, which indeed is seen along the coast and eastern Washington and Oregon (Fig 4a), although it is below the 95% significance test. However, weaker precipitation is found in western Washington and Oregon, which cannot be explained by large scale atmospheric circulation variations.

During the cold ENSO episodes, the north part of the ridge is significantly weakened by a low centered in southwestern Canada (Fig. 5b). Table 2 shows the geopotential height of the ridge decreases by more than 30 m in the Northwest coastal area. This weakening straightens the zonal isobars, intensifies the atmospheric moisture transport from the ocean, and increases the precipitation in the Northwest during the cold ENSO events (Fig. 4b). The amplified precipitation is apparently the reason for the decreased SWE in the Northwest. On the other hand, the southern part of the ridge that is over the ocean is slightly strengthened by the high south of the Aleutian islands. Table 2 shows that the maximum increase of the ridge in this area is less than 17 m. The strengthened ridge increases the northerlies to the Southwest, bringing drier air to the region and reducing the precipitation. Because the ridge is located far to the Southwest, it causes less than a 40mm precipitation reduction, compared to more than a 180 mm precipitation increase in the Northwest due to the dramatically weakened ridge.

Therefore, the SWE anomalies in the WUS are strongly connected to precipitation variations caused by the anomalous atmospheric circulation during the ENSO events. Increased precipitation is found in the Southwest during the warm ENSO, when the ridge located in the North Pacific Ocean is greatly weakened by the low off the coast of North America, increasing the atmospheric moisture transport to the Southwest. Amplified precipitation is seen in the Northwest during the cold ENSO, as the ridge near the coast is greatly reduced by the low centered in southwestern Canada, strengthening the air moisture transport to the Northwestern U.S.

5 Impact of PNA on snowpack in the WUS

Different from the anomalous atmospheric circulation induced by ENSO, PNA pattern is governed by the atmospheric dynamics (Section 3). As presented above, the phases of the PNA pattern are strongly connected with the SWE anomalies in the WUS. During the positive phase of the PNA pattern, the decreased SWE occurs in the entire region, while the increased SWE occurs under the negative PNA pattern. In the following sections, the physical processes between the PNA pattern and SWE anomalies are discussed.

5.1 Precipitation and Temperature

As discussed above, the ENSO episodes change the normal precipitation distribution in the WUS, leading to the SWE anomalies. In a similar fashion, the geographic precipitation and temperature distributions in the WUS under the PNA patterns are examined to understand the SWE anomalies. Fig. 6a shows the precipitation anomalies in the WUS under the positive PNA pattern, which are mostly negative and consistent with the decreased SWEs in the region,

14

although the precipitation areas passing the 95% significance level are not systematically distributed. Meanwhile, during the positive phase of the PNA, the positive temperature anomalies cover almost the entire WUS. The warmer climate results in larger than normal snowmelt during the snow accumulation period, and contributes to the decreased SWEs (Fig. 2c). In Fig.6b, the precipitation has positive anomalies under the negative PNA pattern for most areas of the West, except for the parts of Washington, Wyoming, and New Mexico. At the same time, the temperature has strong negative anomalies. As such, the stronger precipitation and colder temperature lead to the increased SWE (Fig. 2d).

Hence, the atmospheric dynamic-governed PNA patterns produce both precipitation and temperature anomalies in the WUS, leading to the anomalous SWE patterns. However, only the precipitation determines the SWE anomalies during ENSO processes. This partially explains why the PNA induced SWE patterns account for a larger variance of the SWE anomalies (39%) than the ENSO produced SWE patterns (18%).

5.2 500mb geopotential height anomalies during the PNA patterns

The PNA anomaly patterns occur under the normal tropical Pacific SST with periods of significant PNA indices (Fig.7). The differences between PNA and ENSO patterns have been extensively discussed by Strous and Shukla (2002), who indicate that positive PNA patterns are analogous to warm ENSO patterns, and negative PNA patterns correspond to cold ENSO patterns. During the warm ENSO, the high centered over eastern Canada is zonally oriented. However, the high on the positive PNA map shifts to the west coast of North America with a strong meridional orientation. For the warm ENSO, the low centered over the North Pacific Ocean shifts slightly to the west coast of North America, when compared to the positive PNA

15

pattern. This low covers parts of Mexico and the western and southern U.S., extending eastward to Atlantic Ocean. For the positive PNA, the low located in the North Pacific, south of the Aleutian Islands, is cut off by the high over western North America. The warm ENSO generates significant disturbances over the tropical Pacific, but these disturbances are barely seen in the presence of the positive PNA pattern. The cold ENSO and negative PNA anomalous patterns are much more similar than those of the warm ENSO and positive PNA. The only minor differences are that the high, south of the Aleutian Islands for the negative PNA pattern, is stronger than for the cold ENSO, and the height disturbances over the tropical Pacific Ocean for the negative PNA pattern are slightly weaker.

The differences between the patterns of the PNA and ENSO can explain the differences in the surface climate variability resulting from these two processes. On the positive PNA map, a strong high overlaps the entire WUS compared to the mixture of the high and low on the warm ENSO map. The high increases the pressure throughout the WUS, strengthening atmospheric downdrafts in the atmosphere and decreasing cloud fraction. This process results in weaker precipitation and stronger downward solar radiation, thus causing the decreased SWEs in the most areas of the WUS. It can be seen that the northern part of the ridge is located near the center of the high, greatly strengthening the ridge. The variation of the ridge does not cause serious precipitation anomalies, as was found in the ENSO patterns. This is attributed to the meridional structure of the high for the positive PNA pattern, which favors north-south air mass exchanges. The zonal structure of the warm ENSO pattern encourages west-east air mass exchanges between the ocean and the land over the WUS, which has a much stronger moisture gradient than the north-south exchanges as for the positive PNA pattern. This can explain the unsystematically distributed areas of the precipitation anomalies passing the 95% significance test.

For the negative PNA pattern (Fig. 7b), a low covers the WUS except for part of New Mexico. This low encourages upward air motion that strengthens cloud formation. Consequently, the enlarged cloud fraction weakens downward solar radiation to the surface, decreasing the surface temperature and potentially increasing the precipitation. As such, increased snowpack occurs in the WUS under the negative PNA pattern. Although a low covers most of the WUS for both the negative PNA and cold ENSO maps, the SWE distribution is dramatically different. Further examination indicates that the climatological ridge is located on the edge of the low and the transition zone between the low and the high in the mid-latitudes on the negative PNA map. However, on the cold ENSO map, the north part of the ridge is seated near the center of the low, and the southern part is intensified by the high south of the Aleutian Islands. Thus, the ridge's strength has a more pronounced change on the cold ENSO pattern than that on the negative PNA pattern. The strong variation in the ridge's strength for the cold ENSO alters the way that atmospheric moisture is transported to the West, resulting in significant precipitation anomalies. Nevertheless, on the negative PNA pattern, the mild variation in the ridge's height does not generate a serious change in the atmospheric moisture transport between the land and ocean. Thus, stronger precipitation results from intensified lifting of the local available atmospheric moisture triggered by the lower air pressure on the negative PNA pattern. Without the constant atmospheric moisture transport from the ocean, the anomalous precipitation pattern shows an uneven distribution. The above discussion indicates that a small change in large scale atmospheric circulation could lead to a significant variation in regional climate.

Generally, under the PNA patterns, the local pressure variations change the vertical atmospheric flows, resulting in variations in atmospheric conditions, such as cloudiness and incoming solar radiation. The changes in atmospheric dynamics alter the precipitation and

temperature distributions as shown in Figs 6a and b, leading to the SWE anomalies in the WUS. Without extra atmospheric moisture exchange between the land and ocean, as found during the ENSO episodes, the PNA patterns produce weak precipitation anomalies, but strong temperature variations due to the significant local pressure variations.…

6. CCM3 simulations

6.1 SWE anomalies

In this study, the coupled CCM3-SAST simulations are evaluated in the context of understanding SWE anomalies during ENSO episodes and PNA processes through comparison with the observations. Fig 8 shows that the SWE anomaly composites under the simulated ENSO and PNA patterns. These four composites are based on the observed Nino 3.4 and PNA indices (Table 1), which have been applied to the observed snow course data.

Generally, the magnitudes of the CCM3-simulated SWE anomalies are quite small (absolute values are less than 50 mm) compared to observations, which have a maximum absolute value of around 400 mm. Under the simulated warm ENSO pattern, CCM3 produces decreased SWEs (Fig. 8a) in the Northwest, but weaker positive SWE anomalies in New Mexico and Colorado. This is different from the observed pattern (Fig. 2a), where a strong SWE anomaly occurs in the Southwest during the warm ENSO. A detailed examination indicates that the SWE anomalies in the Southwest are less than 10 mm due to a strong warm bias in CCM3 (not shown), leading to little accumulated SWE depth. During the cold ENSO, CCM3-SAST results in increased SWEs in the Northwest, which are similar to observations, because an increased SWE center located in Idaho on the observed map (Fig.2b) is also found on the simulated map. However, but another observed center near the coast of the Northwest is not well simulated by

the model. CCM3-SAST has a weak SWE variation in the Southwest, which is consistent with observations. Under the simulated PNA patterns, although the magnitudes of the SWE anomalies are much lower than observations (Fig. 2c and d), the SWE anomalous patterns are very similar to the observations, where the positive PNA pattern produces decreased SWE over the entire WUS, while the negative PNA pattern generates an increased SWE. In order to understand these snow anomaly simulations in the WUS, the simulated anomalous atmospheric circulation during ENSO and PNA processes are discussed.

6.2 Anomalous atmospheric circulation

Figs. 9a and b show that the simulated atmospheric circulation has a reasonable response to tropical Pacific ENSO SST forcing. However, a number of discrepancies remain between the simulations and observations. During the warm ENSO, on the simulated map, the high over North America shows a westward shift as compared to the observed map, and covers the entire northwestern U.S. and part of the Southwest. The simulated low over the North Pacific Ocean slightly moves away from the North American west coast, and has a higher intensity than the observations. The Southwest becomes a high to low transition zone on the simulated map, where the variations in 500mb geopotential height are very insignificant, while the observed anomalous 500mb heights, with over 95% significance, covers almost the entire Southwest in the period of the warm ENSO. The simulated climatological ridge slightly shifts to the west, but generally agrees well with observations (Fig.5a). The southern part of this simulated ridge is greatly weakened by the low south of the Aleutian Islands, which directs more atmospheric moisture to the Southwest and increases precipitation (Fig. 10a). These processes are in very good agreement with the observations. However, the intensified precipitation, with over 95% significance in the

Southwest, does not help to produce an extensively increased SWE due to the aforementioned warm bias. Meanwhile, the displaced high over North America covers the entire Northwest region on the simulated map of 500 mb geopotential height anomalies, while the high only shields the eastern part in the observation map. The shifted high creates the weaker precipitation and higher surface air temperature in the Northwest, leading to a lower simulated SWE centered in Idaho. However, observed decreased SWE anomalies (Fig. 2a) only appear in the eastern part of the Northwest as a response to the higher pressure.

For the cold ENSO, the low centered over southwestern Canada on the observed map of the 500mb height anomalies dramatically moves to southeastern Canada (Fig. 9b), and the center of the high over the North Pacific Ocean shifts slightly to the west coast of North America, when compared to observations. Despite the displacement of the simulated atmospheric circulation, most areas of the WUS are still in control of the negative 500mb geopotential height anomalies, which is consistent with the observations. However, the magnitudes are lower than the observed values. The lower pressure produces the colder temperature in the WUS (Fig.10d), and does not extensively generate the positive precipitation anomalies with significance above 95% (Fig.10b). Therefore, the decreased SWE in the Northwest is largely attributed to the colder temperature, but for the observations, it is determined by the precipitation, as discussed earlier. Nevertheless, the simulated snowpack in the Southwest does not change significantly, because there is not much snow accumulation in the model over this region. A small area of precipitation reduction is seen in southern California, resulting from the strengthening of the southern part of the climatological ridge by the high south of the Aleutian Islands. However, this precipitation reduction does not seem to reduce the SWE in this area because it is balanced by the colder temperature at the same location.

Figs. 9c and d indicate that CCM3-SAST produces good simulations for the PNA patterns when compared to observations. A high covers the entire WUS for the positive PNA pattern, and a low controls this region under the negative PNA pattern, although the position of the climatological ridge is not quite accurate. The simulated high creates higher temperature (not shown), resulting in a shallower snowpack in the West (Fig.8c), while the low generates lower temperature (not shown), leading to a deeper snowpack (Fig. 8d). The precipitation related to the PNA patterns is very random and unsystematic. Thus, the SWEs under the simulated PNA patterns are largely dependent on the temperature, but are determined by both precipitation and temperature on the observations.

In general, CCM3 coupled to the advanced land surface model SAST (Jin et al. 1999), provides very promising simulations of the large scale atmospheric circulation. However, a minor shift in the large scale circulation would cause a significant change in the surface climate at the regional scale. Especially, the very complex topographies and climate processes in the WUS need be accurately described by a regional climate model with a finer spatial resolution and more sophisticated physics than those in the current version of CCM3.

7. Discussions and conclusions

This paper investigates the impact of the atmospheric circulation in the mid-latitudes on the SWE in the WUS. The anomalous mid-latitude atmospheric circulation is divided into two categories: one is forced by the tropical Pacific ENSO SSTs, and the other is derived from the non-linear dynamics of the atmosphere. Observed Nino-3.4 and PNA indices are applied to construct the ENSO and the PNA patterns. If the standard deviation of the winter Nino-3.4 index is greater than 1°C, based on a 47-year historical record (1950-1997), the corresponding

atmospheric pattern is defined as the warm ENSO pattern. When Nino-3.4 SST is less than -1°C, then the corresponding atmospheric pattern is defined as the cold ENSO pattern. The PNA patterns are constructed under the normal tropical Pacific SSTs. If the PNA index is greater than 0.5, the atmosphere has a positive PNA pattern, while if it is less than -0.5, the atmosphere has a negative PNA pattern. The composite number for each pattern is shown in Table 1. The method for abstracting the ENSO pattern is still problematic due to the small sample number for each ENSO phase (8 for the warm phase and 6 for the cold phase). It is fortunate that our abstracted ENSO patterns are quite consistent with those discussed in Strous and Shukla (2002) and Hoerling et al. (2001). As such, although the resulting ENSO patterns are still influenced by natural variability in the atmosphere, they do not affect the conclusions in this paper.

The warm ENSO exerts a major influence on the Southwest region, leading to decreased SWEs, while the cold ENSO gives increased SWEs in the Northwest. A decreased SWE is seen in the entire WUS under the positive PNA pattern, and an increased SWE is found in the same region under the negative PNA pattern. The EOF analysis of the SWE in the WUS indicates that the ENSO and PNA related snow anomalies account for 57% of the total variance explained in the SWE, with the PNA explaining 39%, and the ENSO explaining 18%. This finding suggests that the PNA patterns play a more significant role in affecting the SWE anomalies in the WUS than the ENSO-induced patterns.

The two major variables affecting SWE accumulation, precipitation and surface air temperature, were examined to understand the snow anomalies in the WUS ENSO-related anomalous precipitation patterns are very consistent with the snow anomalies . During the snow accumulation period, the warm ESNO generates stronger precipitation in the Southwest, and the cold ENSO produces more vigorous precipitation in the Northwest. The variation in precipitation

is strongly connected with changes in the climatological 500mb geopotential height ridge located in the Pacific North America sector. During the warm ENSO phase, the southern part of the ridge (south of 40°N) is significantly weakened by the low that is located in the northern Pacific Ocean, directing more atmospheric moisture to the Southwest and amplifying the precipitation. During the cold ENSO phase, the northern part of the ridge (north of 40°N) is weakened by the low located in North America, leading to more atmospheric moisture transport to the Northwest, resulting in increased precipitation. Additionally, the zonal structure of the ENSO patterns favor west-east airflow exchanges, where a significant moisture gradient exists over regions between the land and the ocean. The temperature has a secondary effect on the SWE anomalies in the WUS, because its anomalous patterns are not quite compatible with those for the SWE anomalies.

A high seated in North America on the positive PNA pattern produces a warmer climate and reduced precipitation over the entire WUS, resulting in a decreased SWE. Meanwhile, a low centered in the middle part of Canada on the negative PNA pattern brings about a colder climate and enhanced precipitation, leading to an increased SWE on the ground. As discussed, the variation in the climatological 500mb geopotential height ridge over the Pacific-North America sector is tightly related to the precipitation anomalies as found on the ENSO patterns. However, under the positive PNA, this ridge is greatly strengthened, but the precipitation variation is very mild when compared to the ENSO cases. Due to its meridional structure, the positive PNA pattern favors the north-south atmospheric moisture exchanges, which have a smaller moisture gradient than the west-east exchanges in the west coast region (as shown on the ENSO patterns). Thus, precipitation does not change significantly under the meridional structure of the positive PNA pattern, although the strength of the climatological ridge increases dramatically. However,

the negative PNA pattern does not apparently bear a meridional structure, especially the portion covering the WUS. Basically, its shape is quite compatible with that of the cold ENSO pattern. Nevertheless, the variation in the climatological ridge on the negative PNA pattern is weaker than that for the cold ENSO pattern due to the slight eastward shift of the low seated in North America, reducing atmospheric moisture exchange between the land and the ocean in the WUS, leading to a mild change in precipitation. The temperature variations under the negative PNA and cold ENSO patterns, which are largely dependent on the local pressures, are quite similar. As such, in spite of the similarity of the cold ENSO and negative PNA patterns, their effects on the surface climate variables in the WUS, such as SWE or precipitation, are dramatically different due to the variations in the climatological ridge.

CCM3 gives very good simulations for the anomalous circulation patterns induced by ENSO and non-linear atmospheric dynamics. However, the model does not simulate the anomalous snowpack pattern very well for the warm ENSO case due to the warm bias in the Southwest and the shifted atmospheric circulation. In the case of the cold ENSO, although the resulting anomalous snowpack patterns in the WUS are consistent for both the simulation and observation, the SWE anomalies result from the temperature variation in CCM3, while they are caused by the anomalous precipitation for the observation. These differences are attributed to the strength of the climatological ridge, which is seen to be greatly weakened on the observed map, but has only a mild change in the simulation map. Under the simulated PNA patterns, the anomalous SWE patterns are in good agreement with the observations. However, the observed SWE anomalies are determined by both precipitation and temperature, and the simulated anomalies are caused only by temperature. The model does not give reasonable precipitation simulations during the PNA processes. Generally, CCM3 produces weaker SWE anomalies in

the WUS than observations. The CCM3 simulations strongly suggest that regional climate simulations need more accurate model physics and higher spatial resolution than those in current AGCMs, because small shifts in large scale circulation would possibly cause significant differences in surface climate at a regional scale.

References

Bonan, G. B., 1996: The NCAR Land Surface Model (LSM version 1.0) coupled to the NCAR Community Climate Model. NCAR Tech. Note NCAR/TN-429+STR, 171pp. [Available from NCAR, P.O. Box 3000, Boulder, CO 80307.]

Bohr, G. S., and E. Aguado, 2001: The use of April 1 SWE measurements as estimates of peak seasonal snowpack and total cold season precipitation. *Water Resour. Res.*, **37**, 51-60.

Cayan, D.R., 1996: Interannual climate variability and snowpack in the western United States. *J. Climate*, **9**, 928-948.

Changnon, D., T.B. Mckee, and N.J. Doesken, 1993: Annual snowpack patterns across the Rockies: Long-term trends and associated 500-mb synoptic patterns. *Mon. Wea. Rev.*, **212**, 633-647.

Clark, M.P., M.C. Serreze, and G.J. McCabe, 2001: The historical effect of El Nino and La Nina events on the seasonal evolution of the montane snowpack in the Columbia and Colorado River basins. *Water Resour. Res.*, **37**, 741-756.

Dettinger M. D., and D. R. Cayan, 1995: Large-Scale atmospheric forcing of recent trends towards early snowmelt runoff in California. *J. Climate*, **8**, 606-623.

Dickinson, R.E, A. Henderson-Sellers, and P.J. Kennedy, 1993: Biosphere Atmosphere Transfer Scheme (BATS) Version 1e as Coupled to the NCAR Community Climate Model. NCAR Technical Note, NCAR/TN-387+STR, 72 pp. [Available from NCAR, P.O. Box 3000, Boulder, CO 80307-3000.]

Grant, L.O., and A.M. Kahan, 1974: Weather modification for augmenting orographic precipitation. *Weather and Climate Modification*, W.N. Ness, Ed., John Wiley and Sons, 282-317.

Groisman, P. Ya., T. R. Karl, and R. W. Knight, 1994: Observational impact of snow cover on the heat balance and the rise of continental spring temperatures. *Science*, **263**, 198-200.

Hoerling, M. P., and A. Kumar, and T. Xu, 2001: Robustness of the nonlinear climate response to ENSO's extreme phases. *J. Climate*, **14**, 1277-1293.

Jin, J., X. Gao, Z. Yang, R. C. Bales, S. Sorooshian, R.E. Dickinson, S. Sun, and G. Wu, 1999: One-dimensional snow water and energy balance model for vegetated surfaces. *Hydrological Processes*, **13**, 2467-2482.

Lau, N.-C., and M. J. Nath, 1994: A modeling study of relative roles of tropical and extratropical SST anomalies in the variability of the global atmosphere-ocean system. J. Climate, **7**, 1184-1207.

Legates, D. R., and C. J. Willmott,1990a: Mean seasonal and spatial variability in global surface air temperature. *Theor. Appl. Climatol.,* **41**, 11-21.

Legates, D. R., and C. J. Willmott,1990b: Mean seasonal and spatial variability in gauge-corrected global precipitation. *Int. J. Climatol.*, **10**, 111-127.

Livezey, R. E., and K. C. Mo, 1987: Tropical-extratropical teleconnections during the Northern Hemisphere winter. Part II: Relationships between monthly mean Northern hemisphere circulation patterns and proxies for tropical convection. *Mon. Wea. Rev.*, **115**, 3115-3132.

Marshall, S., and R. J. Oglesby, 2003: The predicbility of winter snow cover over the western Unitet States. *J. Climate*, **16**, 1062-1073.

McCabe, G.J., and M.D. Dettinger, 2002: Primary modes and predictability of year-to-year snowpack variations in the western United States from teleconnections with Pacific Ocean climate. *J. Hydrometerology*, **3**, 13-25.

McCabe, G.J. and D.M. Wolock, 1999: General-circulation-model simulations of future snowpack in the western United States. *J. American Water Resources Association*, **35**(6),1473-1484.

McCabe, G. J., 1996: Effects of winter atmospheric circulation on temporal and spatial variability in annual streamflow in the western United States. *J. hyrol. Sci*., **41**, 873-887.

Miller, N.L., K.E. Bashford, and E. Strem: Potential impacts of climate change of California hydrology. *J. Amer. Water Resourc. Assoc*, **39**, 771-784.

Serreze, M.C., M.P. Clark, R.L. Amstrong, D.A. McGinnis, and R.S. Pulwarty, 1999: Characteristics of WUS snowpack from SNOTEL data. *Water Resour. Res.*, **35**, 2145-2160.

Strous, D. M., and J. Shukla, 2002: Does ENSO force the PNA. *J. Climate*, **15,** 2340-2358.

Trenberth, K. E., 1997: The definition of El Niño. *Bull. Ameri. Meteor. Soc.*, **78**, 2771-2777.

Wallace, J. M., and D. S. Gutzler, 1981: Teleconnections in the geopotential height field during the Northern Hemisphere winter. *Mon. Wea. Rev*., **109**, 784-812.

Watson .D., 1992: A guide to the analysis and display of spatial data. Pergamon Press, 1992. ISBN 0-08-040286-0.

Captions:

Fig. 1 The 47-year time series of averaged SWE (mm) over the 246 snowcourse stations in the WUS for 1951- 1997. The solid line represents the regressed line for SWE.

Fig.2 1 April snow anomalies for a) the warm ENSO, b) the cold ENSO, c) the positive PNA pattern, and d) the negative PNA pattern. The shaded areas pass the 95% Student's t test. The thick solid contour is the zero anomaly line. The contour interval for the ENSO patterns is 50mm, and for PNA pattern is 30mm. The dashed lines are for negative values, and the solid lines are for positive values.

Fig. 3 EOF loadings for the SWE anomalies in the WUS: a) The loadings for the first EOF component with 39% of the total variance in the snowpack, and b) the loadings for the second EOF component with 18% of the total variance. The contour interval is 0.03.

Fig.4 Precipitation anomalies for: a) warm and b) cold ENSO. The contour interval is 30mm. The 2m height air temperature anomalies for: c) warm and d) cold ENSO. The contour interval is 0.2 $^{\circ}$C. The thin solid lines represent negative contours, the thin dashed lines represent positive contours, and the thick solid line is for the zero anomaly. The anomalies were averaged over November through March.

Fig.5 500mb geopotential height anomalies for: a) the warm ENSO and b) the cold ENSO. The shaded areas pass the 95% Student's t test. The contour interval is 8m. The thin solid lines represent negative contours, and the thin dashed lines represent positive contours. The thick solid

line is for the zero anomaly, and the thick dashed line is for the climatological ridge. The anomalies were averaged over November through March (5 month).

Fig.6 As in Fig.4, but for the PNA patterns.

Fig.7. As in Fig.5, but for the PNA patterns.

Fig.8 As in Fig.2, but for the CCM3 output in March, and the contour interval is 10mm.

Fig.9 As in Fig.5, but for both ENSO and PNA patterns from the CCM3 output.

Fig.10 As in Fig. 4, but for the CCM3 output.

Table 1 Warm and cold ENSO winters, and positive and negative PNA winters, as well as their corresponding indices according to the definitions given in section 3.

ENSO				PNA			
Warm years	Nino-3.4 index (^{o}C)	Cold years	Nino-3.4 index	Positive years	Index	Negative years	Index
1957/58	1.69	1955/56	-1.04	1952/53	0.76	1951/52	-0.57
1965/66	1.38	1970/71	-1.59	1960/61	0.86	1956/57	-0.90
1968/69	1.03	1973/74	-1.77	1962/63	0.67	1964/65	-0.90
1972/73	1.72	1975/76	-1.53	1963/64	0.92	1971/72	-1.66
1982/83	2.68	1984/85	-1.19	1969/70	1.08	1978/79	-0.75
1986/87	1.32	1988/89	-1.83	1976/77	1.30	1981/82	-0.57
1991/92	1.91			1977/78	0.95		
1994/95	1.07			1980/81	1.09		
				1985/86	0.98		

Table 2 Height variations of the climatological ridge at different latitudes over the Pacific/North sector during the ENSO episodes.

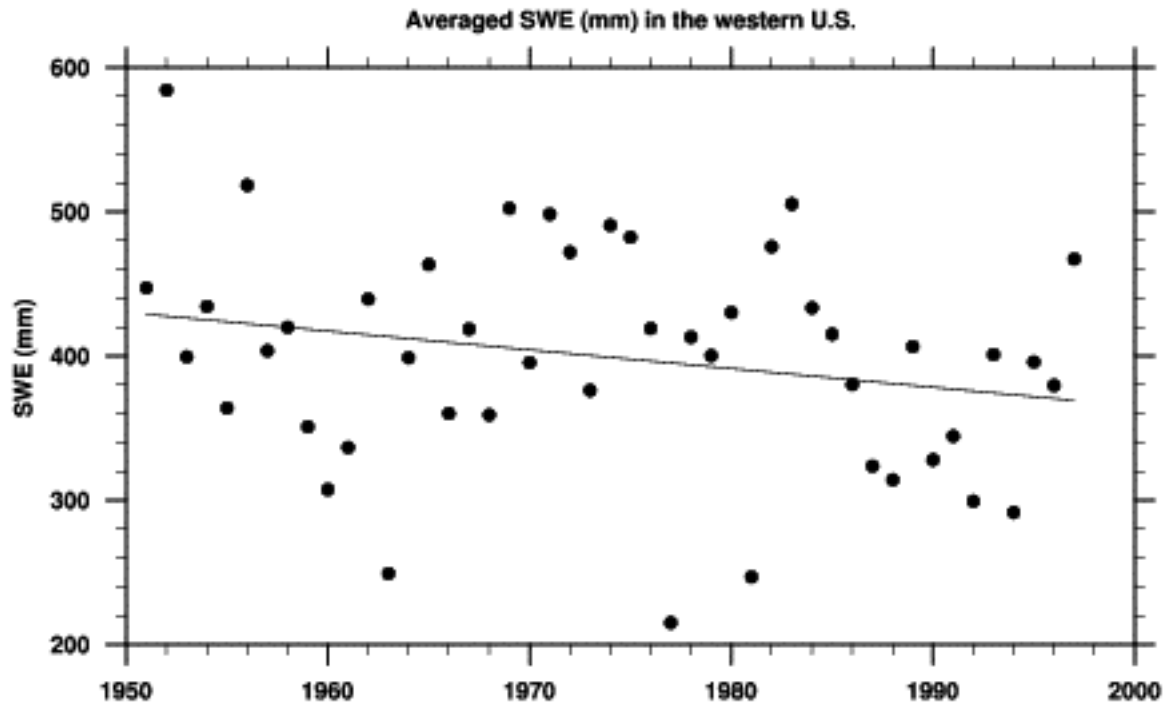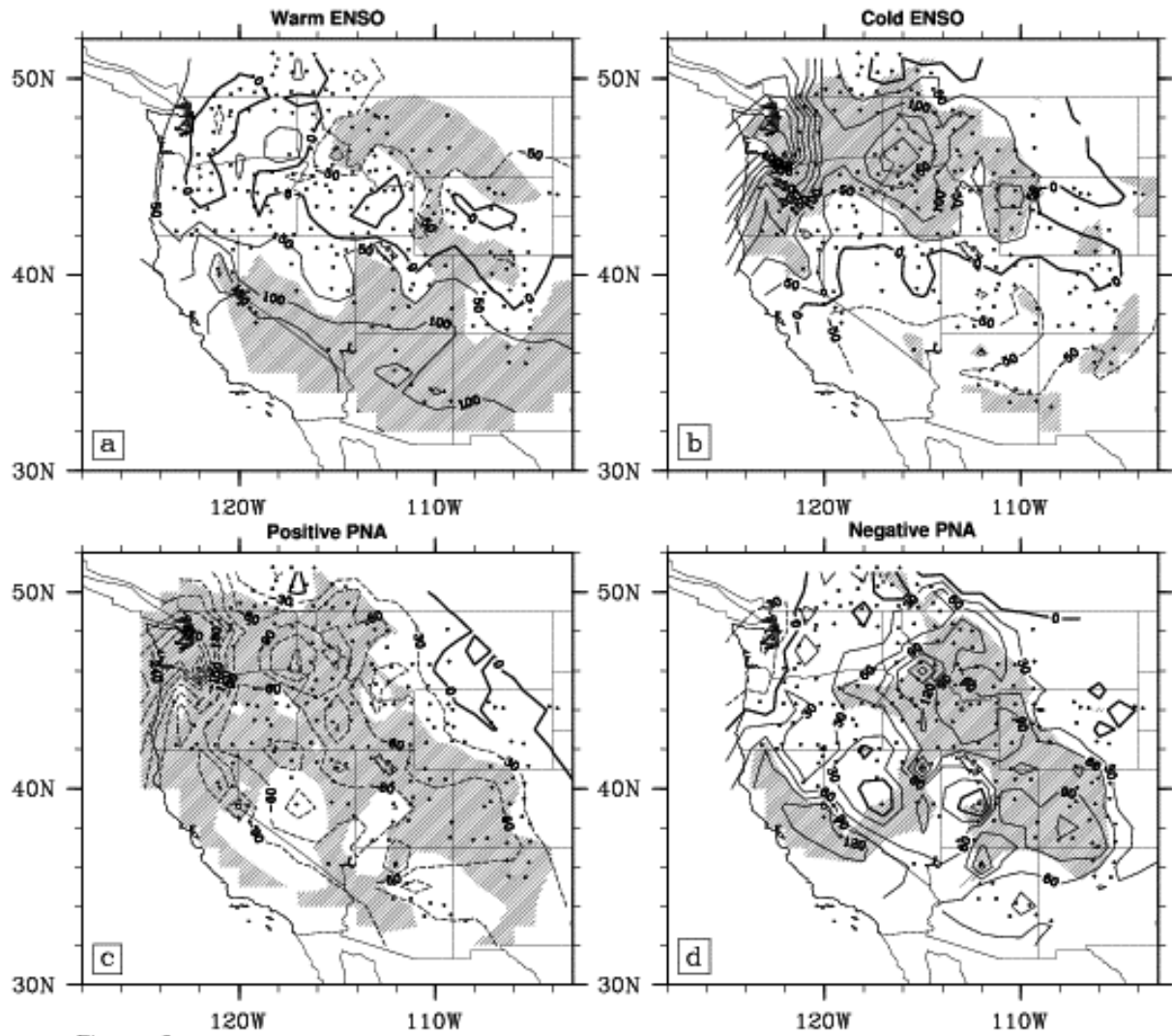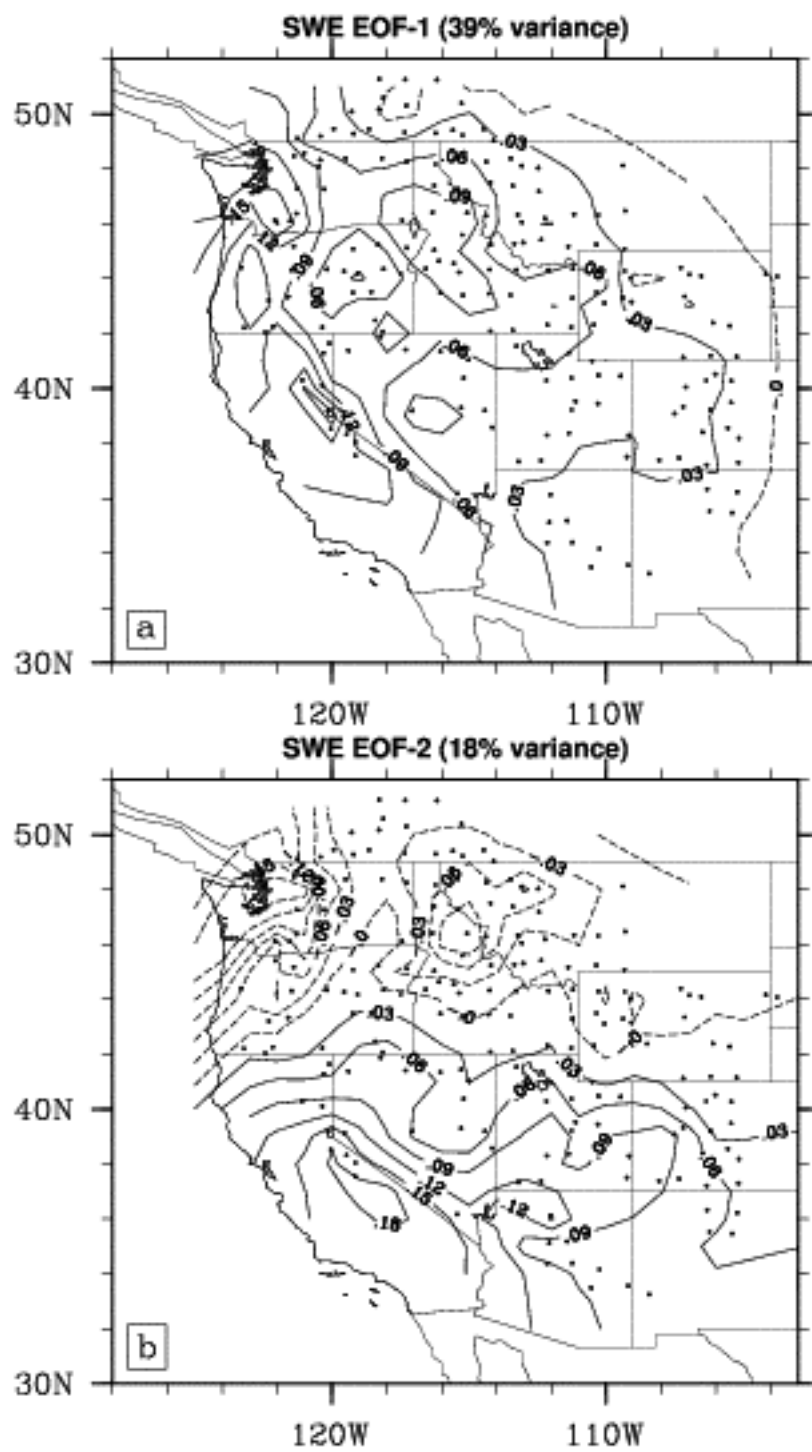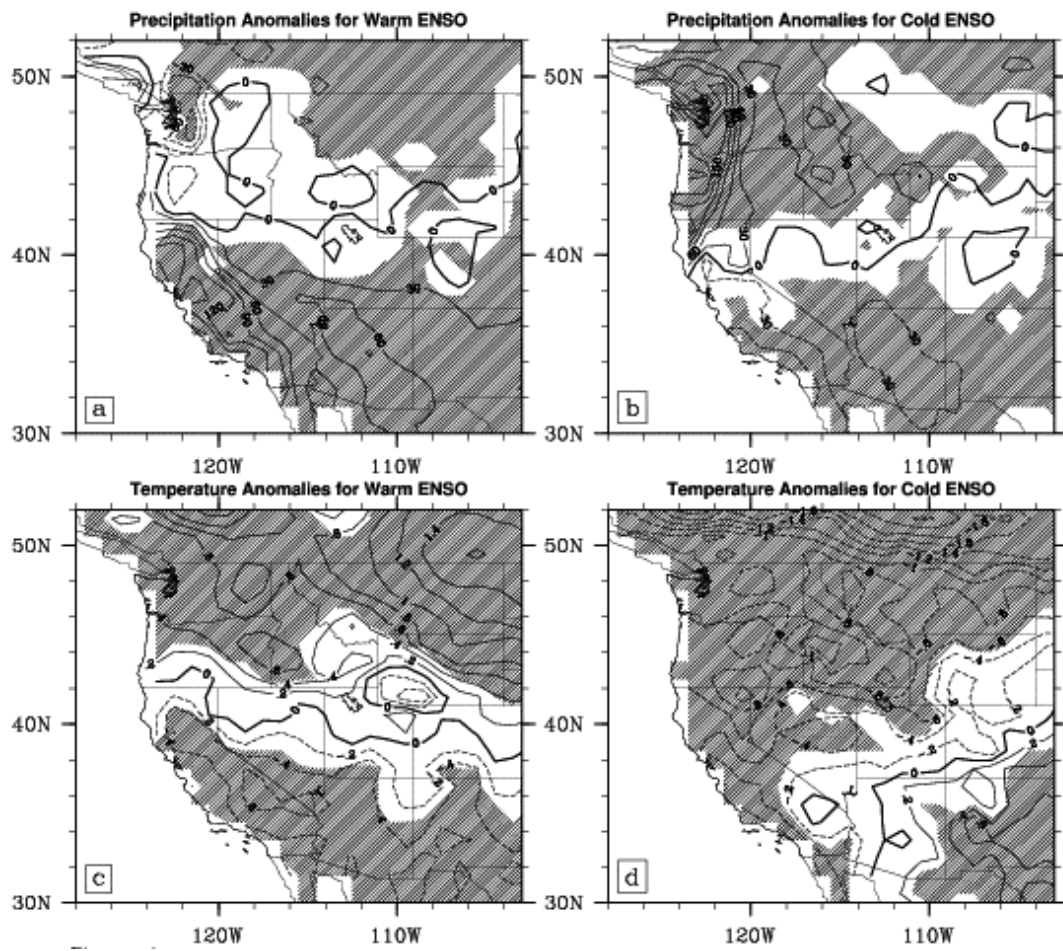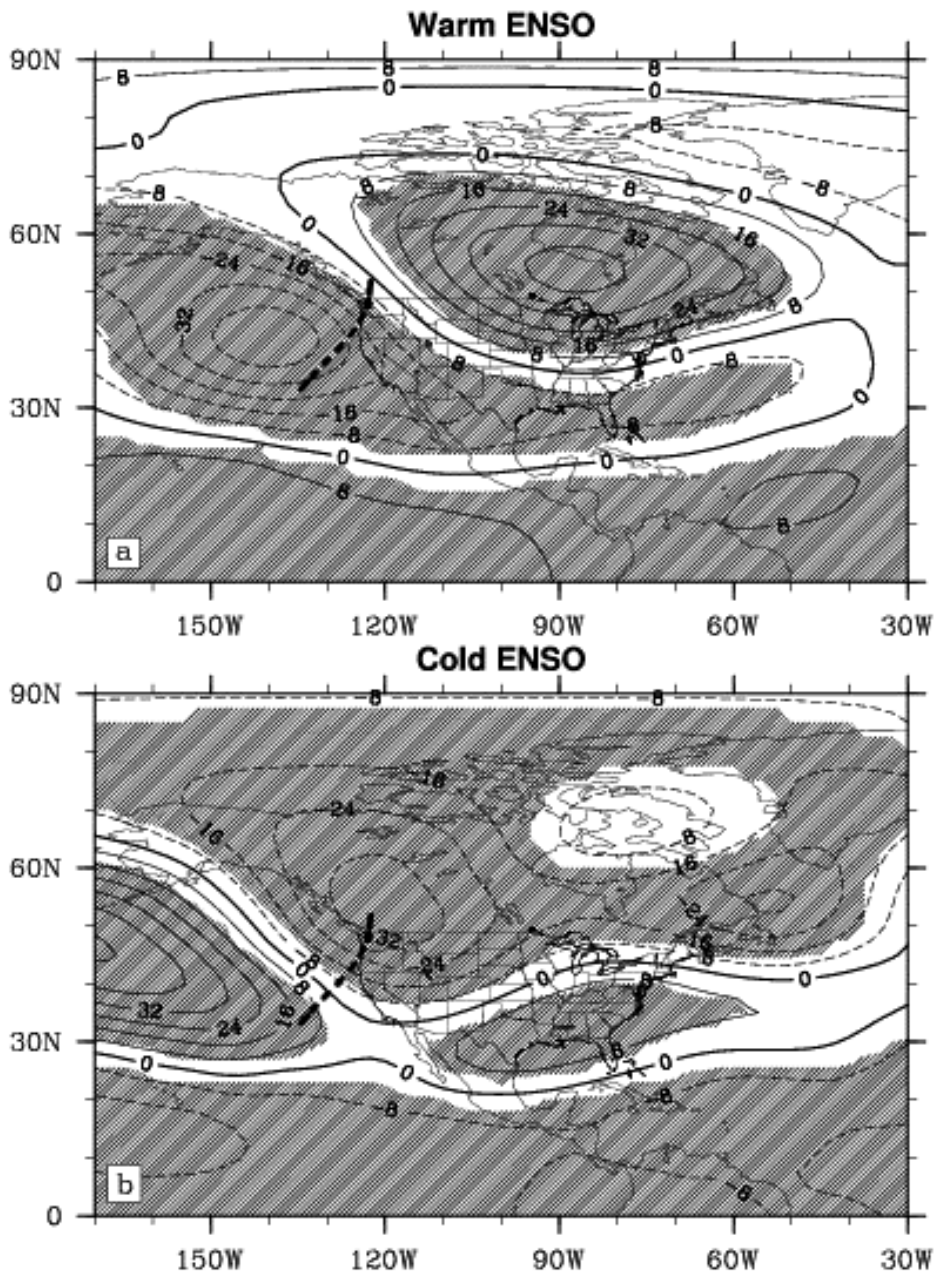| Lat (^{o}N)	Warm ENSO (m)	Cold ENSO (m)
30	-19.4	13.9
32.5	-26.8	16.9
35	-32.1	16.9
37.5	-34.5	12.6
40	-28.1	4.4
42.5	-18.1	-9.8
45	-11.0	-25.1
47.5	-4.6	-31.0
50	0.7	-34.1
52.5	4.1	-35.8
55	6.0	-35.5

Averaged SWE (mm) in the western U.S.

Fig. 1.

Fig. 2.

Fig. 3.

Fig. 4.

Warm ENSO

Cold ENSO

Fig. 5.

Precipitation Anomalies for Positive PNA (mm)

Precipitation Anomalies for Negative PNA (mm)

Temperature Anomalies for Positive PNA (°C)

Temperature Anomalies for Negative PNA (°C)

Fig. 6.

Fig. 7.

Fig. 9.

CCM3 Precip Anomalies for Warm ENSO

CCM3 Precip Anomalies for Cold ENSO

CCM3 Temp Anomalies for Warm ENSO

CCM3 Temp Anomalies for Cold ENSO

Fig. 10